Role of lone pair electrons in determining the optoelectronic properties of BiCuOSe

S. Sallis and L. F. J. Piper*
Department of Physics, Applied Physics and Astronomy, Binghamton University, Binghamton, New York 13902, USA

J. Francis and J. Tate
Department of Physics, Oregon State University, Corvallis, Oregon 97331, USA

H. Hiramatsu, T. Kamiya, and H. Hosono
Materials and Structures Laboratory, Tokyo Institute of Technology, Mailbox R3-1, 4259 Nagatsuta-cho, Midori-ku, Yokohama 226-8503, Japan

(Received 13 December 2011; published 16 February 2012)

The electronic structure of the oxychalcogenides LaCuOSe and BiCuOSe has been studied using O K-edge x-ray emission spectroscopy, x-ray absorption spectroscopy, and density functional theory, in order to examine the effects of the M^{3+} ion configurations. The known distortion of the BiO layers in BiCuOSe compared to the LaO layers in LaCuOCh; the significantly smaller band gap of BiCuOSe (0.9 eV) compared to LaCuOSe (2.8 eV); and similar hole transport properties of the two compounds are explained in terms of the electron lone pairs associated with the Bi $d^{10}s^2p^0$ electronic configuration. The Bi 6s orbitals are chemically active and form bonding and antibonding states with the oxygen 2p orbital. The structural distortion facilitates the interaction between the 6p orbital with 6s via the antibonding state. For BiCuOSe, the majority of the Bi 6s orbital character (i.e., the bonding state) lies below the valence band, with the antibonding state lying below the valence band maximum (VBM). The similar hole transport properties between the two compounds is a consequence of the Bi 6s contributing little to the Cu 3d–Se 4p derived VBM. Finally, the band gap narrowing of BiCuOSe compared to LaCuOSe is mostly due to the low energy of the unoccupied Bi 6p orbitals along with the upshift of the VBM due to the presence of the O 2p–Bi 6s antibonding states.

DOI: 10.1103/PhysRevB.85.085207 PACS number(s): 71.20.Nr, 78.70.En, 78.70.Dm

I. INTRODUCTION

The layered quaternary oxychalogenides MCuOCh (M = trivalent lanthanide ion; Ch = chalcogen ion), consisting of alternating $(M_2O_2)^{2+}$ and $(Cu_2Ch_2)^{2-}$ layers along the c axis, exhibit the unique optoelectronic properties of both optical transparency (band gap energy $E_G \sim 3$ eV) and p-type conductivity.[1] In these materials, the valence band maximum (VBM) has both Cu 3d and Ch np character and the conduction band minimum (CBM) is derived from the Cu 4s orbital. As a result, the optoelectronic properties are determined chiefly by the $(Cu_2Ch_2)^{2-}$ layers; as highlighted by the lack of remarkable differences along the lanthanide series (La ~ Nd, except for Ce).[2] These oxychalcogenides display superior hole conductivities compared to the Cu oxide delafossites with narrow Cu 3d derived VBM, due to the chalcogenide p character at the VBM. Indeed, the conductivities of LaCuOCh were found to increase upon going down the chalcogenide group in accordance with greater orbital overlap between the Cu 3d and Ch np orbitals.[3]

The use of a nonlanthanide trivalent pnictogen Bi^{3+} has prompted interest due to BiCuOCh being structurally equivalent to layered LaCuOCh, but with a stable $d^{10}s^2p^0$ configuration. Heavier post-transition ions (Tl^+, Pb^{2+}, Bi^{3+}), with psuedoclosed $6s^2$ shells are thought to form chemically inert and sterically active lone pairs derived from on-site mixing of nonbonding cation s and p orbitals facilitated by a structural distortion (i.e., a pseudo Jahn-Teller distortion which gives rise to a directional s-p hybrid orbital. A classic example is α-PbO, where all four coordinated oxygen atoms are found on one side of Pb with the lone pair on the opposite side. Earlier studies have shown that while Bi^{3+} and La^{3+} have similar ionic radii, the BiO layers in BiCuOCh were more distorted (i.e., smaller O-metal-O bond angles) compared to LaO layers in LaCuOCh; with the BiO layers having the same structure as α-PbO.[3] Density functional theory (DFT) calculations of PbO[4,5] and SnO[6,7] revealed that 6s orbital is *not* chemically inactive, but hybridizes with the O 2p orbital to form bonding (B) and antibonding (AB) states near the bottom and top of the valence band, respectively. This was experimentally confirmed by O K-edge x-ray emission spectroscopy (XES) and hard x-ray photoemission spectroscopy (HAXPS) for a range of post-transition metal oxides.[8] In the revised lone-pairs model framework, the distortion of the crystal facilitates the interaction between the cation 6s–oxygen 2p AB level and the nominally empty cation p states, resulting in the directional lone-pair character.[9] Moreover, the relative energy of the cation s and anion p states is critical to the formation of stereochemically active lone pairs, thus explaining the general trend of lone-pair active oxides and nonactive chalcogenides (S, Se, Te).[9–11]

In the case of clinobisvanite $BiVO_4$ (Bi^{3+}), the filled Bi 6s–O 2p AB state at the VBM[12] resulted in improved p-type conductivity (by providing shallow acceptor levels,[13] and a reduced hole effective mass[14]) with a reduced band gap compared to other polymorphs without lone-pair distortions.[15] By analogy, the peusdo-closed-shell $6s^2$ configuration of Bi^{3+} should result in similar differences between BiCuOSe and LaCuOSe. Recent DFT calculations of BiCuOSe have indicated that the Bi 6s orbital does hybridize with the O

$2p$ orbital to form B and AB states near the bottom and top of the valence band (but *below* the Cu $3d$-Ch np derived VBM), respectively.[3,16] The distortion of the crystal facilitates the interaction between the Bi $6s$–O $2p$ AB level and mostly empty cation p states, resulting in the directional lone-pair character (as shown graphically in Ref. 16). The lack of significant AB character at the Se $4p$ (and Cu $3d$) VBM would support the observed similar conductivities reported between LaCuOCh and BiCuOCh.[3] The smaller band gap of BiCuOSe (0.8–0.9 eV)[3,17] is consistent with a smaller energetic separation between the the Bi $6s$–O $2p$ AB level and the mostly empty cation p states further compounded by the VBM lying above the AB states.

Here, we employ a combination of bulk-sensitive O K-edge XES and corresponding x-ray absorption spectroscopy (XAS) to examine the electronic structure of BiCuOSe, with direct comparison to LaCuOSe, in order to study the effect of the lone-pair formation. Strict on-site dipole selection rules ensure that only electrons with O $2p$ character are involved in the transition, and consequently the intensity is directly proportional to the O $2p$ character. O K-edge XES has been shown to be a simple and direct means of establishing the extent of the hybridization of the Bi $6s$ and O $2p$. Indeed, O K-edge XES was used to first examine the nature of heavy metal lone pairs (i.e., Tl, Pb, and Bi with N-2 oxidization states, where N is the valence) by confirming the interaction between the metal s^2 and O $2p$ states in the valence band (i.e., the formation of bonding states below the valence band) predicted by DFT.[8] Likewise, O K-edge XAS can be used to study transitions from the O $1s$ core-level to unoccupied states with O $2p$ character [i.e., the *partial* density of states (PDOS)]. The O K-edge XAS of metal oxides is well known to map mainly the unoccupied electronic structure at the metal sites, due to hybridized states above the Fermi level with mostly metal weight and some O $2p$ character. As a result, it has been routinely used to determine the conduction band electronic structure of metal oxides (e.g., Ref. 18). In this manner, we directly compare our experimental results with DFT calculations to explain the origin of the optoelectronic properties and structural distortion of BiCuOSe in terms of oxygen mediated lone-pair formation.

II. EXPERIMENT

Epitaxial thin films of nominally undoped (∼100-nm thick) LaCuOSe were prepared on MgO (001) single-crystal substrates via reactive solid-phase epitaxy.[19] Their structural and optoelectronic properties can be found elsewhere.[3,20] The BiCuOSe samples were also grown on MgO substrates by pulsed laser deposition.[21,22] Trace amounts of Ca were expected from the growth of these films but the Ca signal was below the detection limit of XPS measurements.

X-ray spectroscopy measurements were performed at beamline X1B at the National Synchrotron Light Source (NSLS), Brookhaven National Laboratory. The beamline is equipped with a spherical grating monochromator and a Nordgren-type grazing-incidence spherical grating spectrometer. The emission measurements of the O K edge were performed in a near-specular geometry and were carried out using a spectrometer resolution of 370 meV (or better) with an incident photon energy well above threshold (540 eV). The energy axes were calibrated from Zn metal $L_{\alpha,\beta}$ emission lines measured in the second order of diffraction during the same experiment. The Cu $L_{\alpha,\beta}$ emission in the second order of diffraction was clearly observed for the XES detector settings used to measure the O K edge. This provided a means of optimizing the sample positions by maximizing the signal from the epitaxial film in order to reduce any spectral contamination from the oxide substrates. The corresponding XAS spectra were recorded in total electron yield (TEY) mode by measuring the nanoampere current variation from the sample, and were normalized to the current from a reference Au-coated mesh in the incident photon beam. The energy resolution was set at 190 meV for the O K edge. The energy scale of the XAS measurements was calibrated using first- and second-order diffraction Ti $L_{3,2}$ edge absorption features of rutile TiO_2. For direct comparison with the experimental data, DFT periodic calculations were performed using the VASP code[23] with the projector augmented wave (PAW) method[24,25] using PBE96 generalized gradient approximation (GGA) functionals. Further details can be found elsewhere.[20] The calculated band gaps were 0.3 and 1.5 eV for BiCuOSe and LaCuOSe, respectively. The calculations are summarized in Fig. 1. To consider the effects of the instrumental resolution, the calculated PDOS have been Gaussian broadened to approximate the resolution settings used for the XES and XAS measurements (i.e., full width at half maximum of ∼0.4 and 0.2 eV, respectively.

III. RESULTS

Figure 2 displays the O K-edge XES and XAS on the same common photon energy plot for both the BiCuOSe and LaCuOSe. The combination of the O K-edge XES and XAS can be employed to deduce the bulk fundamental gap between the occupied (XES) and unoccupied (XAS) states of metal oxides. The spectra are referenced to the O $1s$ core level (i.e., 528.9 eV below the Fermi level). The valence and conduction band edges were determined from the second derivatives.[26,27] In Fig. 2 we show the least-square fits to the spectra using Gaussian functions. The band edges are identified as the peaks in the second derivatives of the topmost valence band (XES) and bottommost conduction band (XAS) Gaussian peaks in Fig. 2, which yielded band edge separations for BiCuOSe and LaCuOSe of 0.3 and 2.2 eV, respectively. It is immediately apparent that the BiCuOSe displays a significantly narrower gap than LaCuOSe, consistent with optical measurements.[3] It is important to consider the different final states of the XES and XAS process in order to be quantitative. The core-hole final state of the XAS results in a shift to lower photon energies reducing the apparent band gap when referenced to the XES. Although the shift is less significant for O K-edge absorption (∼0.5–1 eV) than for the transition metal L edges (∼5 eV), it still needs to be accounted for. Applying a core-hole shift of 0.6 eV for both spectra resulted in band edge separation values which compare well to 0.9 and 2.8 eV from optical measurements reported elsewhere.[3,17] Since the spectra are referenced to the O $1s$ core level, we can clearly consider the band gap differences of BiCuOSe compared to LaCuOSe as due to the combined upshift of the VBM and lowering of the CBM. We note that a core-hole shift is an approximation, but a value of

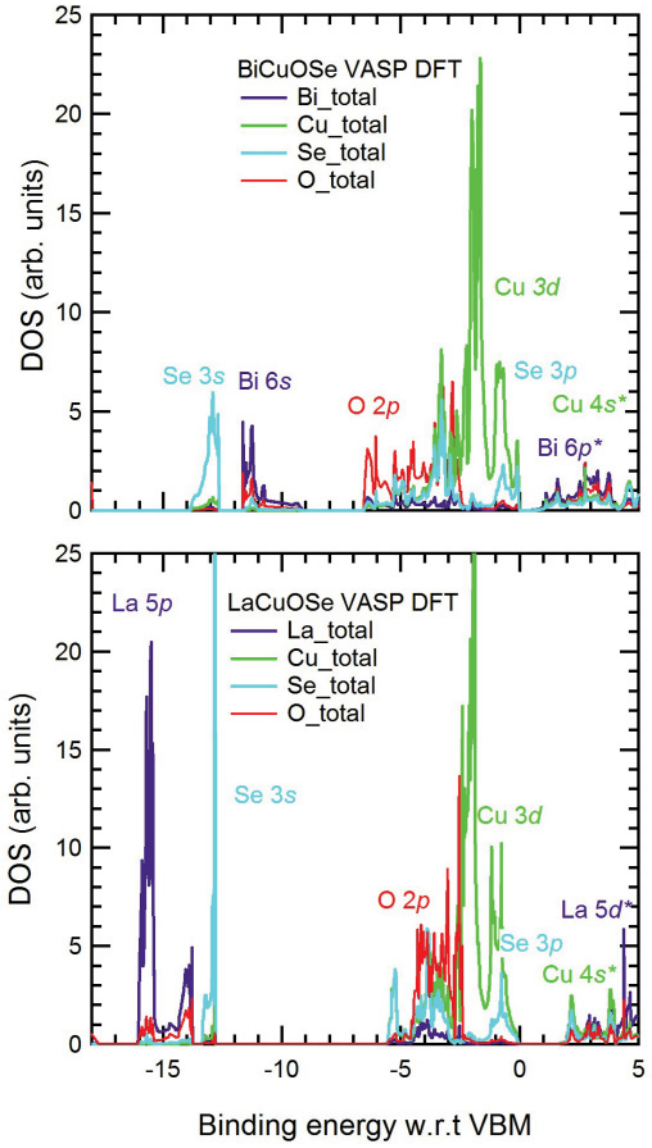

FIG. 1. (Color online) (Top) The DFT calculated PDOS of the valence and conduction band regions of BiCuOSe. The energy axis is referenced with respect to the VBM, such that zero eV is the VBM. The major orbital contribution is highlighted; the * denotes unoccupied orbital state. (Bottom) The corresponding calculated PDOS for LaCuOSe.

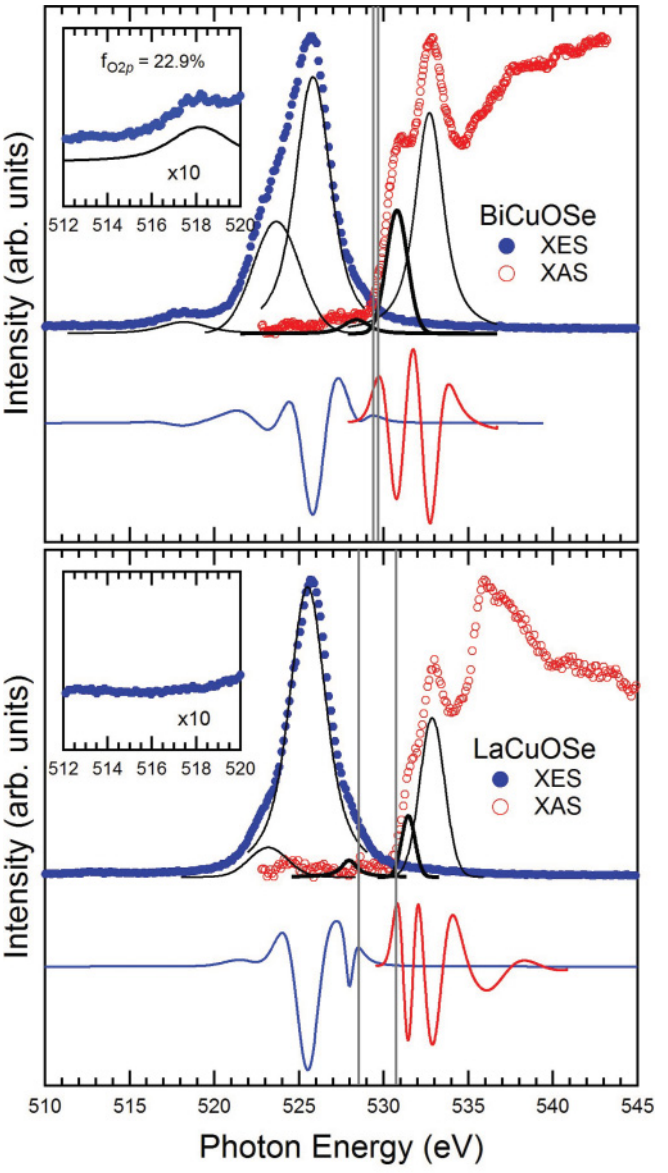

FIG. 2. (Color online) (Top) BiCuOSe O K-edge XES (solid circles) and core-hole corrected XAS (open circles) data plotted against the second derivatives (underneath) of the corresponding least-squares fits (lines). The separation between the band edges is shown (vertical dashed lines), as determined from the separation of the maxima of the second derivatives. The inset displays a magnified region of the XES and corresponding peak fit associated with O 2p–Bi 6s bonding state. (Bottom) The corresponding plot for LaCuOSe; note the lack of spectral weight in the inset.

$\sim$1 eV has been successfully applied to ZnO[28] and $BiVO_4$.[12] Applying a rigid core-hole shift of 0.6 eV would correspond to equal amounts of VBM raising and CBM lowering in BiCuOSe compared to LaCuOSe. Regardless of the exact choice of core-hole value, it is clear that the band gap reduction of BiCuOSe (compared to LaCuOSe) is due to both band edges evolving.

The direct comparison between the emission spectra and the corresponding Gaussian-broadened O 2p PDOS from DFT calculations (shifted by the O 1s core level) is plotted in Fig. 3 (along with the corresponding occupied Bi 6s and La 5p PDOS for comparison). The calculated VBM have been rigidly shifted to agree with the experimentally determined VBM from our spectra. Near the top of the valence band region (i.e., $>$525 eV) the two compounds display near identical spectral weight and shape both experimentally and theoretically. The calculations reveal that for both compounds the topmost region is primarily Cu 3d and Se 4p character, with the majority of the O 2p orbital lying $\sim$3–6 eV below the VBM and only a slight contribution from Bi 6s orbitals near/at the VBM. At $\sim$3 eV below the VBM the valence band character of the two compounds differs significantly, with BiCuOSe having increased spectral weight at higher binding energies and an additional peak below the main valence band region (at $\sim$11 eV below the VBM). The general shape of the Gaussian-broadened DFT nicely reproduces the experimental spectra, with the least-squares fits mimicking the broadened

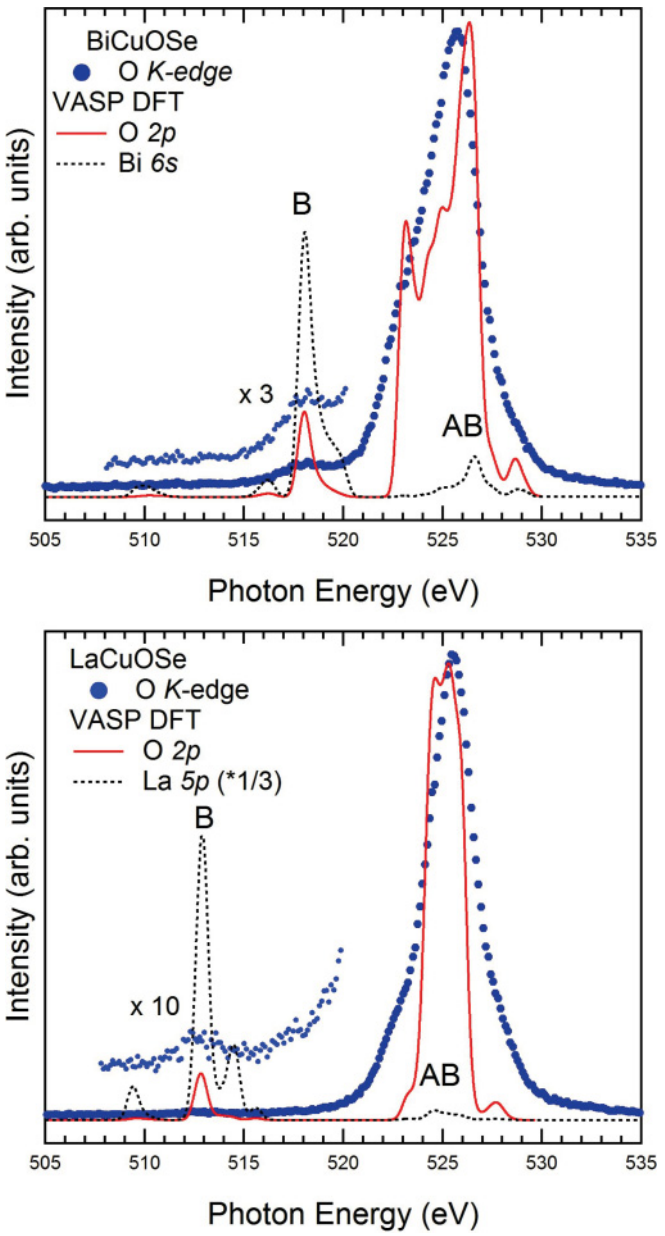

FIG. 3. (Color online) (Top) BiCuOSe XES data plotted against Gaussian broadened DFT calculated O $2p$ and Bi $6s$ PDOS. The DFT has been rigidly shifted for the calculated VBM (zero binding energy) to match the experimentally determined VBM at 529.38 eV (photon energy). (Bottom) LaCuOSe XAS data plotted against the Gaussian broadened O $2p$ and La $5p$ PDOS, rigidly shifted by 528.54 eV (i.e., to match the experimentally determined VBM of LaCuOSe). The locations of the bonding (B) and antibonding states (AB) are identified in each case.

DFT spectra. The peak fitting ensured that we included the topmost valence band region (i.e., the Cu $3d$–O $2p$ derived VBM) when determining the band edges. Merely extrapolating the leading edge of the O XES to the baseline would not have done so. For BiCuOSe, the Bi $6s$–O $2p$ bonding and antibonding states are predicted to lie below and slightly above the main O $2p$ manifold, respectively. The bonding state is clearly observed in the BiCuOSe emission spectrum at ~11 eV below the VBM (i.e., 518.5 eV), and reproduced in the DFT calculations (both Bi $6s$ and O $2p$). The O $2p$ contribution (f_{O2p}) at the Bi $6s$—O $2p$ bonding peak was determined by comparing the curve-fitted area ratios (A^{peak} and A^{total}) by

$$f_{O2p} = \frac{(A^{\text{peak}}/A^{\text{total}})}{(n/p)}, \tag{1}$$

where n is the number of metal atoms per formula unit and p is the total number of valence electron pairs per formula unit.[8,9] For BiCuOSe, $n = 2$ (Bi and Cu) and $p = 12$ [i.e., half of the total number of valence electrons: d^{10} (Cu^{+}) + s^2 (Bi^{+3}) + p^6 (Se^{2-}) + p^6 (O^{2-})]. This gives an experimental f_{O2p} of 0.23, in fair agreement with the value of 0.31 obtained from our DFT calculations. It also agrees well within the overall trend in f_{O2p} versus group number for the modified lone-pair model.[8] We note the significantly increased O $2p$ weight at energies greater than 526 eV for BiCuOSe compared to LaCuOSe. This would be consistent with the largely oxygen character of the AB state.

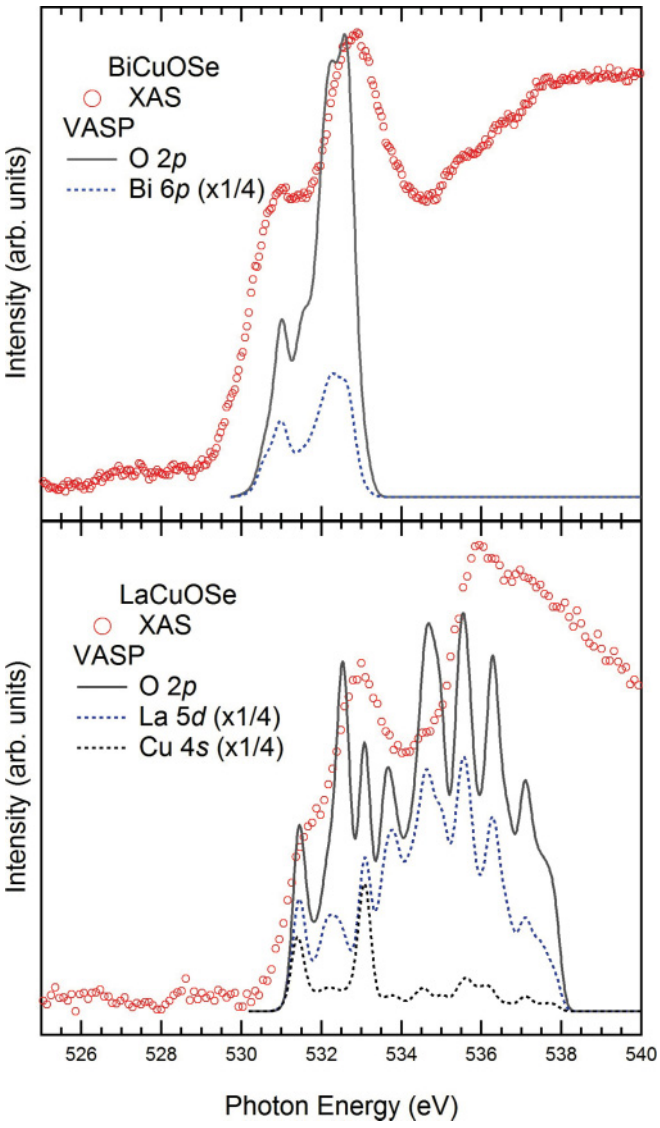

FIG. 4. (Color online) (Top) BiCuOSe XAS data plotted against Gaussian broadened DFT calculations of Bi $6p$ and O $2p$ contributions. (Bottom) LaCuOSe XAS data plotted against Gaussian broadened DFT calculations of La $5d$, Cu $4s$, and O $2p$ contributions.

Our DFT calculations confirm that the AB state lies mostly at ∼3 eV (i.e., 526.5 eV), as highlighted in Fig. 3. At this energy, there is significant mixing between the Bi 6*s*–O 2*p* AB and Bi 6*p* orbital in our DFT calculations, consistent with the revised lone-pairs model.[9] For LaCuOSe we do observe a very weak peak at ∼15 eV below the VBM (i.e., 513.5 eV) in the emission spectrum associated with La 5*p*–O 2*p* B state in agreement with the DFT calculated energy, as shown in Fig. 3. In contrast to BiCuOSe, the corresponding AB state is calculated to lie nearer the bottom of the valence band region (i.e., ∼524 eV) of LaCuOSe, also shown in Fig. 3. The energetic location of Bi 6*s*–O 2*p* AB state is then considered to be responsible for the higher energy of the VBM for BiCuOSe compared to LaCuOSe, contributing to the smaller band gap observed.

The XAS data for BiCuOSe and LaCuOSe are plotted in Fig. 4 alongside the corresponding DFT calculations of the unoccupied O 2*p* PDOS. For direct comparison, we have rigidly shifted the DFT energies for alignment between the calculated VBM and the VBM of the experimental spectra, and then increased the conduction band onset to correct for the underestimation of the calculated band gap. The O 2*p* PDOS reproduces spectral features in both systems. Also included in Fig. 4 are the Bi 2*p* PDOS for BiCuOSe, and the La 5*d* and Cu 4*s* PDOS for LaCuOSe. As expected, the DFT confirms that the unoccupied O 2*p* PDOS is mapping the metal orbitals. It also confirms that the low-lying Bi 6*p* orbital is responsible for lowering the CBM. The low energy of the Bi 6*p* level, due to scalar relativistic effects, is consistent with the modified lone-pairs model which predicts indirect mixing of the AB Bi 6*s*–O 2*p* and Bi 6*p* orbitals through structural distortion.[9]

IV. CONCLUSION

Direct comparison between the experimental spectra of LaCuOSe and BiCuOSe confirms that the origin of the band gap reduction is the raising of the VBM (due to the presence of the AB state) and the lowering of the CBM (due to the Bi 6*p* orbital), with band edge separations from the XES/XAS (core-hole corrected by 0.6 eV) in agreement with the optically measured band gaps of the two compounds. We experimentally confirm the presence of a Bi 6*s*–O 2*p* bonding state just below the valence band, consistent with other lone-pair active Bi^{3+} containing metal oxides.[8,12] Excellent agreement is observed between our experimental spectra and the O 2*p* PDOS calculated within DFT. Our results are consistent with a revised lone pair description,[9] whereby the combination of the low lying Bi 6*p* orbital (due to scalar relativistic effects) and the chemical interaction between the Bi 6*s* and O 2*p* results in the formation of electron lone pairs facilitated by a structural distortion enabling mixing between the Bi 6*p* and Bi 6*s*–O 2*p* states. Little hybridization occurs between the Bi 6*s* and Se 3*p* states (which lie higher in energy than the O 2*p*), resulting in the VBM character of BiCuOSe being similar to LaCuOSe. As a result, the *p*-type transport properties should be similar between the two compounds. In this manner, the optoelectronic differences between LaCuOSe and BiCuOSe can be explained in terms of the formation of Bi 6*s*–O 2*p* lone pairs due to the Bi^{3+} configuration.

ACKNOWLEDGMENTS

The authors thank Professor Kevin Smith for use of his end station at X1B during our allocated beamtime. The National Synchrotron Light Source is supported by the US Department of Energy, Contract No. DE-AC02-98CH10886. L.F.J.P. and S.S. acknowledge support from the Faculty/Student Research Support Program at the NSLS. The Binghamton Research was supported in part by funds from an Advanced Diagnostics Laboratory Small Grant at Binghamton University. The Oregon State research is supported by the National Science Foundation under Grant No. DMR 0804916. The work at the Materials and Structures Laboratory was supported by the Japan Society for the Promotion of Science (JSPS), Japan, through the Funding Program for World-Leading Innovative R&D on Science and Technology (FIRST) Program.

*lpiper@binghamton.edu

[1] H. Hosono, Thin Solid Films **515**, 6000 (2007).
[2] K. Ueda, K. Takafuji, H. Hiramatsu, H. Ohta, T. Kamiya, M. Hirano, and H. Hosono, Chem. Mater. **15**, 3692 (2003).
[3] H. Hiramatsu, H. Yanagi, T. Kamiya, K. Ueda, M. Hirano, and H. Hosono, Chem. Mater. **20**, 326 (2008).
[4] G. W. Watson, S. C. Parker, and G. Kresse, Phys. Rev. B **59**, 8481 (1999).
[5] G. W. Watson and S. C. Parker, J. Phys. Chem. B **103**, 1258 (1999).
[6] A. Walsh and G. W. Watson, Phys. Rev. B **70**, 235114 (2004).
[7] G. W. Watson, J. Chem. Phys. **114**, 758 (2001).
[8] D. J. Payne, R. G. Egdell, A. Walsh, G. W. Watson, J. Guo, P.-A. Glans, T. Learmonth, and K. E. Smith, Phys. Rev. Lett. **96**, 157403 (2006).
[9] A. Walsh, D. J. Payne, R. G. Egdell, and G. W. Watson, Chem. Soc. Rev. **40**, 4455 (2011).
[10] A. Walsh and G. W. Watson, J. Phys. Chem. B **109**, 18868 (2005).
[11] A. Walsh and G. W. Watson, J. Solid State Chem. **178**, 1422 (2005).
[12] D. J. Payne, M. D. M. Robinson, R. G. Egdell, A. Walsh, J. McNulty, K. E. Smith, and L. F. J. Piper, Appl. Phys. Lett. **98**, 212110 (2011).
[13] W. J. Yin, S. H. Wei, M. M. Al-Jassim, J. Turner, and Y. Yan, Phys. Rev. B **83**, 155102 (2011).
[14] A. Walsh, Y. Yan, M. N. Huda, M. M. Al-Jassim, and S.-H. Wei, Chem. Mater. **21**, 547 (2009).
[15] A. Kudo, K. Omori, and H. Katol, J. Am. Chem. Soc. **121**, 11459 (1999).
[16] E. S. Stampler, W. C. Sheets, M. I. Bertoni, W. Prellier, T. O. Mason, and K. R. Poeppelmeier, Chem. Mater. **47**, 10009 (2008).
[17] A. P. Richard, J. A. Russell, A. Zakutayev, L. N. Zakharov, D. A. Keszler, and J. Tate, J. Solid State Chem. (in press), doi:10.1016/j.jssc.2011.11.013.
[18] F. M. F. de Groot, M. Grioni, J. C. Fuggle, J. Ghijsen, G. A. Sawatzky, and H. Petersen, Phys. Rev. B **40**, 5715 (1989).
[19] H. Ohta, K. Nomura, M. Orita, M. Hirano, K. Ueda, T. Suzuki, Y. Ikuhara, and H. Hosono, Adv. Funct. Mater. **13**, 139 (2003).

[20]H. Hiramatsu, T. Kamiya, T. Tohei, E. Ikenaga, T. Mizoguchi, Y. Ikuhura, K. Kobayashi, and H. Hosono, J. Am. Chem. Soc. **132**, 15060 (2010).
[21]J. Tate, P. F. Newhouse, R. Kykyneshi, P. A. Hersh, J. Kinney, D. H. McIntyre, and D. A. Keszler, Thin Solid Films **516**, 5798 (2008).
[22]A. Zakutayev, P. F. Newhouse, R. Kykyneshi, P. A. Hersh, D. A. Keszler, and J. Tate, Appl. Phys. A **102**, 485 (2011).
[23]G. Kresse and J. Furthmüller, Phys. Rev. B **54**, 11169 (1996).
[24]P. E. Blöchl, Phys. Rev. B **50**, 17953 (1994).
[25]G. Kresse and D. Joubert, Phys. Rev. B **59**, 1758 (1999).
[26]B. Gilbert, C. Frandsen, E. R. Maxey, and D. M. Sherman, Phys. Rev. B **79**, 035108 (2009).
[27]S. W. Cho, L. F. J. Piper, A. DeMasi, A. R. H. Preston, K. E. Smith, K. V. Chauhan, R. A. Hatton, and T. S. Jones, J. Phys. Chem. C **114**, 18252 (2010).
[28]A. R. H. Preston, B. J. Ruck, L. F. J. Piper, A. DeMasi, K. E. Smith, A. Schleife, F. Fuchs, F. Bechstedt, J. Chai, and S. M. Durbin, Phys. Rev. B **78**, 155114 (2008).